Optimal dynamic induction and yaw control of wind farms: effects of turbine spacing and layout

Wim Munters and Johan Meyers

Department of Mechanical Engineering, KU Leuven, Celestijnenlaan 300A, B3001 Leuven, Belgium

E-mail: wim.munters@kuleuven.be, johan.meyers@kuleuven.be

Abstract. Turbine wake interactions in wind farms result in decreased power extraction in downstream rows. The current work investigates dynamic induction and yaw control of wind farms for increased total power extraction. Six different wind farm layouts are considered, and the relative benefits of induction control, yaw control, and combined induction–yaw control are compared. Preliminary results show that, through coordinated induction control, turbine density can be increased significantly with the same wind-farm efficiency as an uncoordinated farm.

1. Introduction

Turbine wake interactions in wind farms result in decreased power extraction in downstream rows. The promise of increasing total power extraction through coordinated wind-farm control has incited a multitude of studies into axial induction control and yaw control of wind turbines. In earlier work [1, 2], a dynamic induction control approach was introduced based on large-eddy simulations (LES) and optimization, and analysis of the optimization results led to the identification of a sinusoidal induction control strategy for first-row turbines [3]. Recently, the dynamic optimal control approach was expanded to also include yaw [4]. A control study of a 4×4 wind farm with 6 rotor diameters spacing illustrated that yaw control tends to be more favorable than induction control for small sets of aligned wind turbines, and that combining yaw and induction control potentially further increases power gains.

In the current work, we aim to quantify and compare the potential power gains for induction control, yaw control and combined induction–yaw control in large wind farms with both aligned and staggered layouts. Especially in the latter, the abovementioned advantage of yaw control over induction control is expected to be diminished, since yaw could lead to detrimental interactions between different columns of wind turbines by transversally deflected turbine wakes. Furthermore, control studies are also performed for wind farms with an increased turbine density, where the effect of turbine wake interactions on wind-farm power is further increased.

The paper is structured as follows. Firstly, Section 2 elaborates on the optimal control methodology used in this study. Next, Section 3 details the case setup. Subsequently, Section 4 presents the results of the optimization cases. Finally, Section 5 formulates general conclusions and provides suggestions for further research.

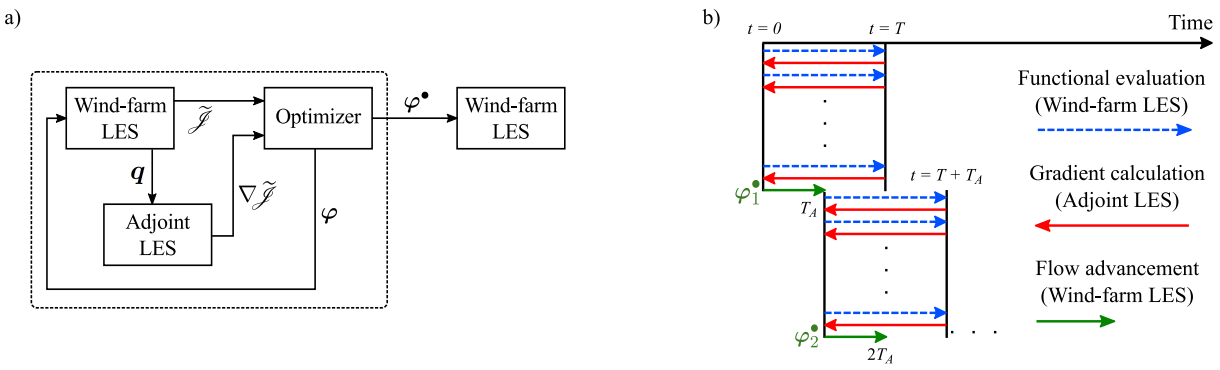

Figure 1: Schematic overview of wind-farm optimal control methodology. *a)* Control block diagram with adjoint gradient-based optimization and LES flow models illustrating data flow of (optimal) controls $\boldsymbol{\varphi}^{(\bullet)}$, system state $\boldsymbol{q}$, cost functional $\mathscr{J}$ and its gradient $\nabla\mathscr{J}$. *b)* Receding horizon framework subdividing time into discrete flow advancement windows of length T_A with prediction horizon T. Each arrow represents a forward or adjoint LES. Every window consists of an optimization stage (blue and red lines) follow by a flow advancement stage with optimal controls $\boldsymbol{\varphi}^{\bullet}$ (green lines). Figure adapted from Ref. [3] (published under a CC BY-4.0 license).

2. Methodology

The current section provides a brief description of the optimal control methodology used in the current paper. A more detailed description of the methodology can be found in Refs. [1, 2, 4]. Figure 1 provides a general overview of the methodology. Figure 1a illustrates the control block diagram: the wind-farm control vector $\boldsymbol{\varphi}(t)$ is optimized until a set of optimal control $\boldsymbol{\varphi}^{\bullet}(t)$ is found. The wind-farm flow model consists of a turbulence-resolving LES and the gradient of the cost functional $\mathscr{J}$ (i.e. the total wind-farm power) is evaluated using the continuous adjoint formulation of the forward LES system. In this way, *a priori* simplification of the representation of the boundary layer and turbine wakes is avoided as much as possible, and control signals can be designed to tap into the unsteady dynamics of the turbulent flow.

Figure 1b illustrates the receding-horizon approach to wind-farm control followed in the current work. Wind-farm controls are optimized over a finite time horizon T, resulting in a number of alternating LES and adjoint LES simulations, after which the optimized controls $\boldsymbol{\varphi}^{\bullet}(t)$ are used in a flow advancement simulation with time horizon T_A. Within each window, wind-farm operation is optimized by solving the following constrained optimization problem:

$$\min_{\boldsymbol{\varphi},\boldsymbol{q}} \qquad \mathscr{J}(\boldsymbol{\varphi},\boldsymbol{q}) = -\int_0^T \sum_{i=1}^{N_t} \frac{1}{2}\widehat{C}'_{T,i}\, V_i^3 A_i \mathrm{d}t \tag{1}$$

$$\text{s.t.}\ \frac{\partial\widetilde{\boldsymbol{u}}}{\partial t} + \left(\widetilde{\boldsymbol{u}}\cdot\nabla\right)\widetilde{\boldsymbol{u}} = -\nabla(\widetilde{p}+\widetilde{p}_\infty)/\rho - \nabla\cdot\boldsymbol{\tau}_{sgs} + \sum_{i=1}^{N_t}\boldsymbol{f}_i \qquad \text{in } \Omega\times(0,T], \tag{2}$$

$$\nabla\cdot\widetilde{\boldsymbol{u}} = 0 \qquad \text{in } \Omega\times(0,T], \tag{3}$$

$$\tau\frac{\mathrm{d}\widehat{C}'_{T,i}}{\mathrm{d}t} = C'_{T,i} - \widehat{C}'_{T,i} \qquad i = 1\ldots N_t \text{ in } (0,T], \tag{4}$$

$$\frac{\mathrm{d}\theta_i}{\mathrm{d}t} = \omega_i \qquad i = 1\ldots N_t \text{ in } (0,T], \tag{5}$$

$$C'_{T,\min} \le\ C'_{T,i} \le C'_{T,\max} \qquad i = 1\ldots N_t \text{ in } (0,T], \tag{6}$$

$$-\omega_{\max} \le\ \omega_i \le \omega_{\max}. \qquad i = 1\ldots N_t \text{ in } (0,T], \tag{7}$$

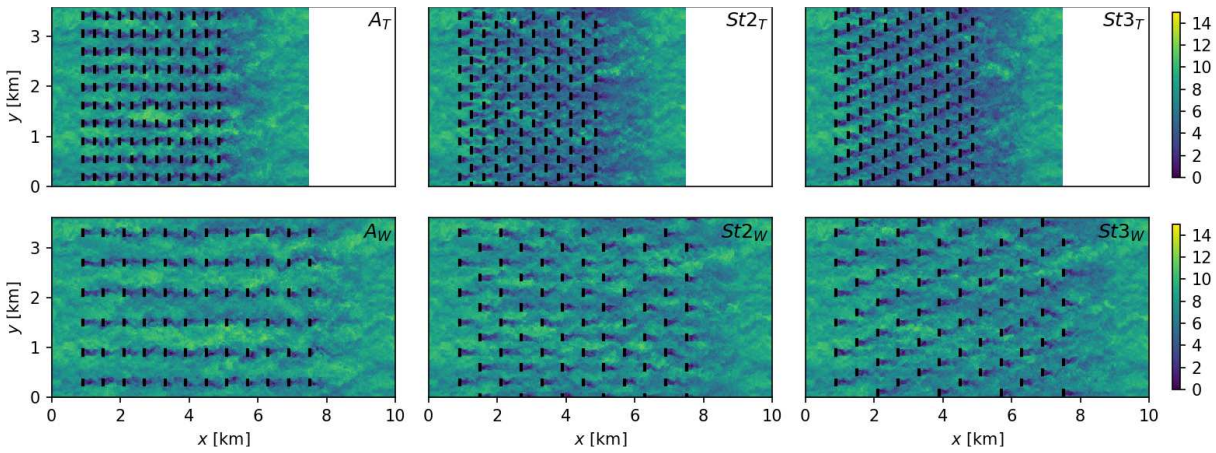

Figure 2: Wind-farm layouts: (A) Aligned, (St2) Staggered every two rows, (St3) Staggered every three rows. Top: (T) Tight spacing, $S = 3.6D$. Bottom: (W) Wide spacing, $S = 6D$. Colors represent instantaneous streamwise velocity in m s^{-1}.

with system states $\boldsymbol{q}(\boldsymbol{x},t) = [\tilde{\boldsymbol{u}}(\boldsymbol{x},t),\ \tilde{p}(\boldsymbol{x},t),\ \widehat{C}'_{T,1}(t),\ldots,\widehat{C}'_{T,N_t}(t),\theta_1(t),\ldots,\theta_{N_t}(t)]$ and controls $\boldsymbol{\varphi}(t) = [C'_{T,1}(t),\ldots,C'_{T,N_t}(t),\omega_1(t),\ldots,\omega_{N_t}(t)]$. State equations (2 – 3) are the filtered Navier–Stokes equations modeling the turbulent wind-farm boundary layer, which are discretized with a mixed spectral–finite difference in space and a fourth order explicit Runge Kutta schemes in time. In these equations, $\tilde{\boldsymbol{u}}$ and $\tilde{p}$ are the filtered velocity and pressure respectively. Further, $\nabla\widetilde{p}_\infty$ is the driving background pressure gradient and $\boldsymbol{\tau}_{\text{sgs}}$ is the subgrid-scale stress tensor. The thrust force $\boldsymbol{f}_i$ enacted on the flow by each turbine i is modeled using an actuator disk approach as $\boldsymbol{f}_i = \frac{1}{2}\widehat{C}'_{T,i}V_i^2\mathscr{R}_i\boldsymbol{e}_{\perp,i}$, with $\widehat{C}'_{T,i}$ the thrust coefficient, $\mathscr{R}_i$ the geometric footprint of the turbine on the LES grid, and $V_i = (1/A_i)\int_\Omega \mathscr{R}_i\tilde{\boldsymbol{u}}\cdot\boldsymbol{e}_{\perp,i}\mathrm{d}\boldsymbol{x}$ the disk-averaged velocity. The rotor-perpendicular vector $\boldsymbol{e}_{\perp,i} = \boldsymbol{e}_x\cos\theta_i + \boldsymbol{e}_y\sin\theta_i$, with θ_i the turbine yaw angle. The thrust coefficient $\widehat{C}'_{T,i}$ is obtained from its setpoint value $C'_{T,i}$ through an exponential time filter with characteristic turbine response time $\tau = 5$ s (Eq. 4), and the turbine yaw angle is found through integration of the yaw rate ω_i (Eq. 5). Finally, controls are bound to technical box constraints in Eqs. (6 - 7). The optimization problem is solved in a reduced formulation using the gradient-based L–BFGS–B algorithm [5]. As mentioned above, the cost functional gradient is calculated using the continuous adjoint method. A detailed elaboration of the adjoint equations and verification of the adjoint gradient is included in Ref. [4], and is omitted here for brevity.

3. Case Setup

We consider a total of six wind farms, comprised of three layouts with two different spacings. Figure 2 illustrates the wind farms for the aligned (A), two-row staggered ($St2$), and three-row staggered ($St3$) cases. For each of these layouts, a tight (T) spacing and wide (W) spacing arrangement is considered, with axial and transversal spacings of $S_T = 3.6D$ and $S_W = 6D$ respectively. The tightly and widely spaced farms are simulated with a resolution of $26\times14\times6.9$ m^3 on domains of size $10\times3.6\times1$ km^3 and $7.5\times3.6\times1$ km^3, hence resulting in simulation grids of $384\times256\times144$ and $288\times256\times144$ respectively in axial, transversal and vertical directions. Inflow conditions are the same for all simulation cases and are generated in a separate precursor domain with shifted periodic boundary conditions [**?**] in which a driving pressure gradient of $\nabla\widetilde{p}_\infty/\rho = 2.5\times10^{-4}$ m s^{-2} results in a free-stream velocity $U_\infty \approx 8.5$ m s^{-1} at hub height. Simulations are advanced in time with a constant timestep of $\Delta t = 0.75$ s.

For each farm, four control cases are considered. Firstly, a greedy reference control case (R)

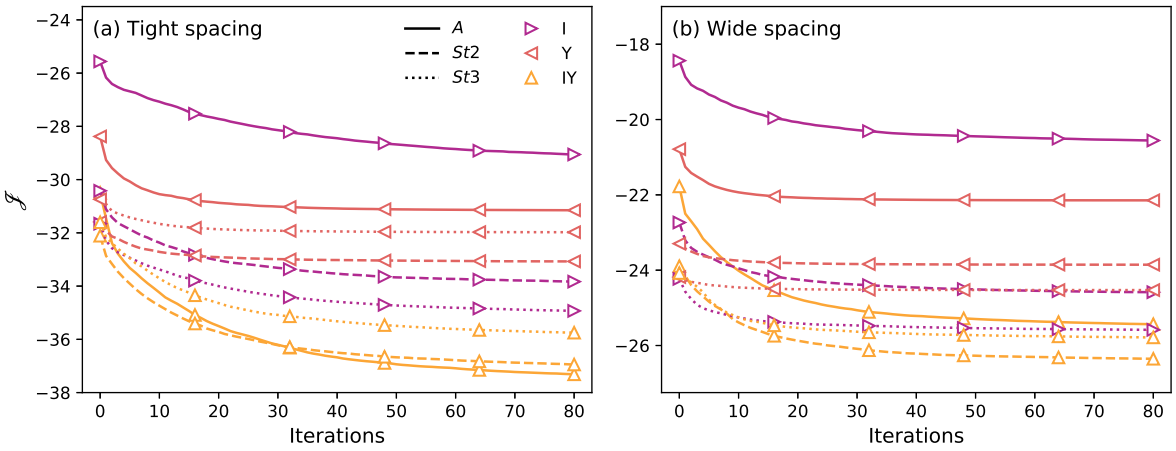

Figure 3: Cost functional decrease in terms of BFGS iterations for all optimization cases in window 6. (a) Tight spacing optimal control cases. (b) Wide spacing optimal control cases. Linestyles indicate the wind-farm layout. Markers (plotted every 15 iterations) indicate the control case.

is defined, in which turbines have a yaw angle fixed perpendicular to the mean-flow direction with steady thrust coefficients $C_T' = 2$, corresponding to the Betz-optimal value. Furthermore, three optimal control cases are investigated: an induction control case, in which turbines remain aligned to the mean flow but the thrust coefficient C_T' can vary between 0 and 3, a yaw control case (Y), in which turbines can yaw at a maximum rate of $\omega_{\max} = 0.3°/\mathrm{s}$ (equal to the NREL 5MW maximum yaw rate [**?**]) with $C_T' = 2$, and a combined induction–yaw control case (IY), with $0 \leq C_T' \leq 3$ and $\omega_{\max} = 0.3°/\mathrm{s}$.

The wind-farm flow fields are simulated over a total time of 18 minutes, consisting of 9 optimization windows with $T = 120$ s and $T_A = T/2 = 60$ s. The L–BFGS–B algorithm is performed for a maximum amount of 80 iterations within each optimization window (see below). For all time-averaged results shown below, the first two windows are omitted to compensate for startup effects due to wake propagation.

4. Simulation Results

The current section discusses the simulation results of the optimal control cases defined in the previous section. Firstly, the choice of the maximum amount of iterations is justified based on the convergence behavior of the optimizations. Thereafter, power extraction and wind-farm efficiency are discussed. Finally, we provide a qualitative view on flow field statistics and control dynamics.

4.1. Convergence Behavior

As mentioned above, optimizations are terminated after 80 optimization iterations. Figure 3 shows the convergence behavior of time window 6 in each optimal control case. It is observed that, although formal convergence is not achieved after 80 iterations for any of the control cases, further improvements in the cost functional are expected to be minimal, and the relative ordering of cases can be assumed to remain the same.

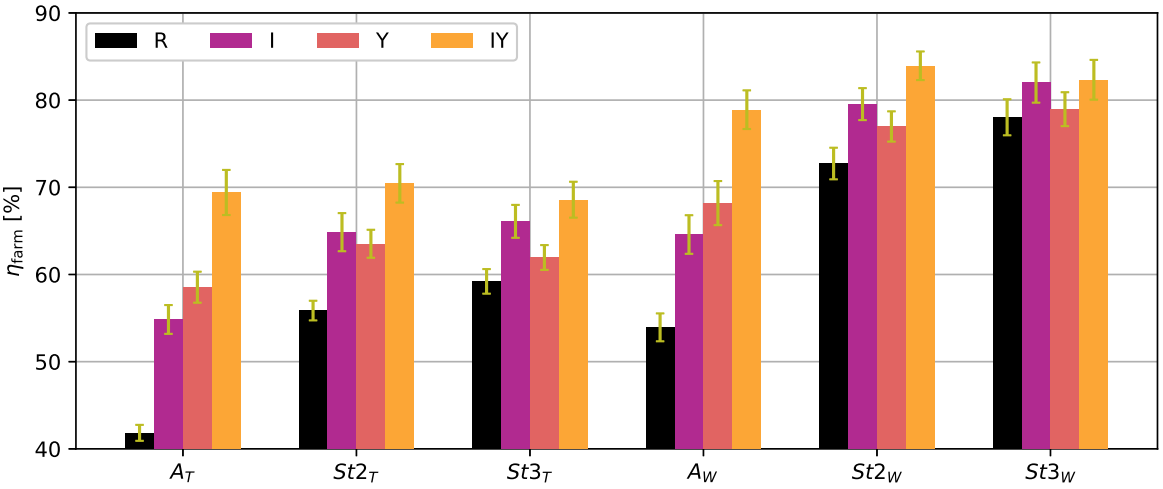

Figure 4: Wind-farm efficiency η_{farm} with respect to a reference case in which every turbine produces the average power of the first-row turbines in the A_T layout. Errorbars indicate confidence intervals of $\pm$ 2 standard deviations and are calculated using the procedure detailed in Appendix C of Ref. [4].

Table 1: Wind-farm efficiencies for all simulation cases, including the relative increase over the greedy reference control cases in brackets.

	Tight			Wide		
	A	$St2$	$St3$	A	$St2$	$St3$
R	0.42	0.56	0.59	0.54	0.73	0.78
I	0.54 [+31%]	0.65 [+16%]	0.66 [+12%]	0.65 [+20%]	0.80 [+9%]	0.82 [+5%]
Y	0.59 [+39%]	0.64 [+14%]	0.62 [+4%]	0.68 [+26%]	0.77 [+6%]	0.79 [+1%]
IY	0.70 [+66%]	0.71 [+26%]	0.69 [+16%]	0.79 [+46%]	0.84 [+15%]	0.82 [+6%]

4.2. Power Extraction and Wind-Farm Efficiency

Figure 4 and Table 1 show the wind-farm efficiency for all simulation cases. A first observation is that the optimal control approach achieves significant power gains in every case except for St3_WY. The latter can be explained by the fact that St3_W already has a relatively high reference efficiency due to its large streamwise turbine spacing and that the turbine placement leaves limited room for increasing power through wake redirection. Furthermore, the improvements in wind-farm efficiency are higher for wind farms with more severe axial wake interactions, i.e. higher for aligned than for staggered layouts, and higher for tight than for wide spacings.

For all layouts except St3_W, the combined yaw and induction controls in case IY significantly outperform separate yaw and induction controls of cases Y and I respectively. Interestingly, when comparing the merits of yaw and induction control, the control strategy with the highest yield is dependent on the wind-farm layout: for aligned wind farms A_T and A_W yaw control allows to achieve higher power extraction than induction control (consistent with the observations by Munters and Meyers [4]), whereas for all staggered cases induction control is slightly more advantageous than yaw control. This shows that the most advantageous control strategy depends on the effective layout of the wind farm, which in turn depends on the mean wind direction, and hence justifies further research into both control strategies.

Row-averaged power extraction is shown in Fig. 5. Panels (a) and (d) illustrate the tightly

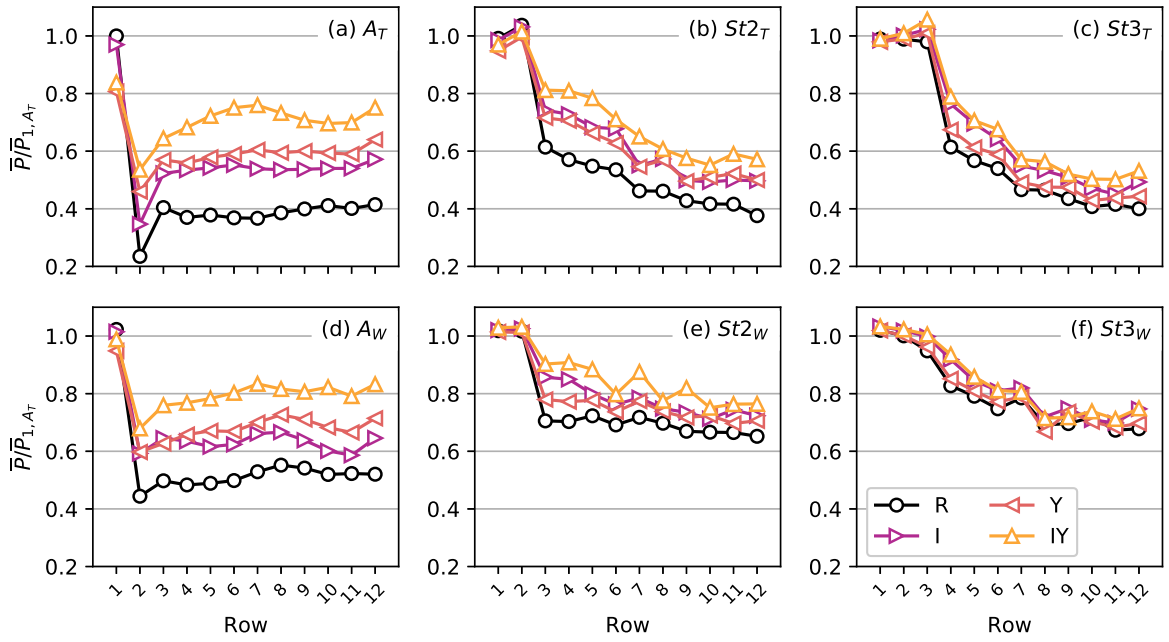

Figure 5: Row-averaged mean power extraction for all simulation cases, normalized by first-row mean power in the reference case of the A_T layout.

spaced and widely spaced aligned layouts respectively, for which is was found that yaw control was more favorable than induction control. It is shown that first-row power is curtailed more for cases Y and IY (involving yaw control) than for case I based on induction, and more so for a tight than for wide turbine spacings, consistent with larger yaw misalignments required to redirect wakes over shorter distances (see further below). Power extraction in downstream rows is in the same range for yaw and induction control, with yaw control achieving higher gains than induction control. The power extraction for the two-row staggered St2 layout in panels (b) and (e) shows power gains for yaw and induction control to lie much closer together throughout the entire wind farm, with a slight advantage for induction control, especially in rows 3 and 4 of the widely spaced layout. Panels (c) and (f) illustrate that, for the three-row staggered St3 layout it is more difficult to significantly increase power extraction over the greedy reference case, with relatively limited gains for induction control and even smaller ones for yaw control.

4.3. Flow Field Statistics and Control Dynamics

The current section discusses the flow field and control dynamics of the different control cases. For brevity and clarity of the discussion, we omit the three-row staggered St3 layout and focus on the aligned A and two-row staggered St2 layout, which exhibit a much larger increase in performance for the optimal control cases.

Firstly, we provide a qualitative illustration of how the optimized controls influence the wind-farm flow field. Figures 6 and 7 show contours of the time-averaged axial velocity at hub height for the tightly and widely spaced wind farms respectively. For clarity of representation, only a selected amount of wind turbine columns are shown.

5. Conclusion

Kanttekeningen: - beperkte totale optimalizatietijd –¿ kan mogelijks de staggered cases wat benadelen voor inductie, of de aligned cases voor yaw - maar dit lijkt de huidige resultaten enkel

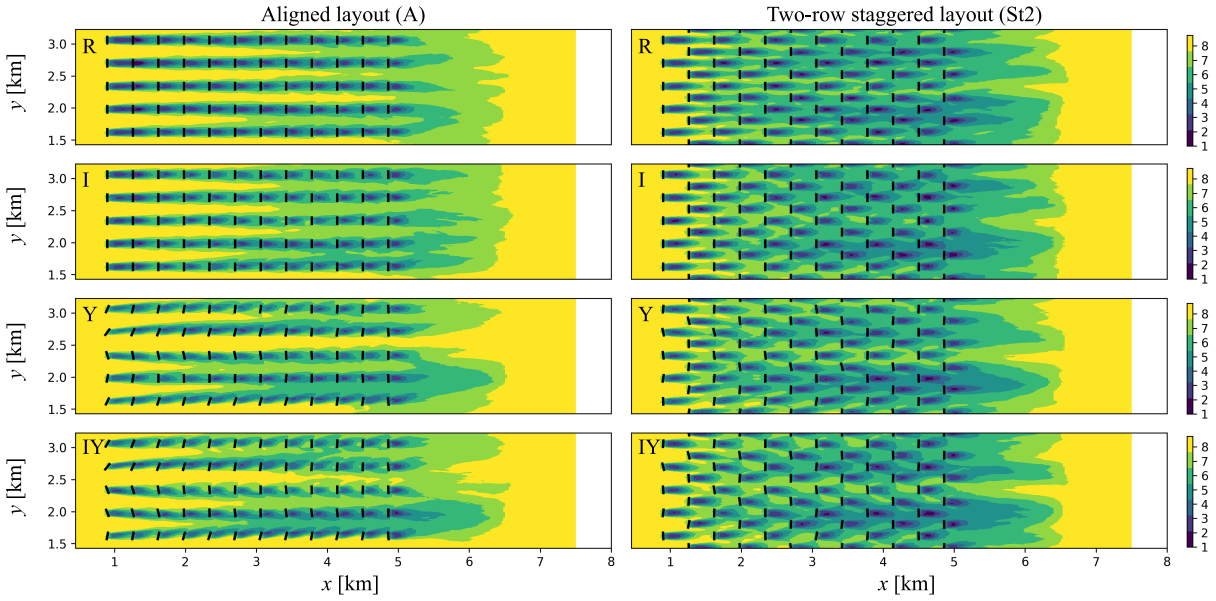

Figure 6: Contours of axial velocity at hub height for tightly-spaced wind farms. Turbine rotors are yawed according to the time-averaged turbine yaw angle. *Left:* Aligned layout. *Right:* Two-row staggered layout. *From top to bottom:* Greedy reference control (R), Induction control (I), Yaw control (Y), Combined yaw and induction control (IY). Coloring is in units of m s^{-1}.

te bevestigen - lokale optima –¿ gegeven onze ervaring met meerdere startpunten - geen formele convergentie –¿ cases zijn vrij goed geconvergeerd (zie figuur)

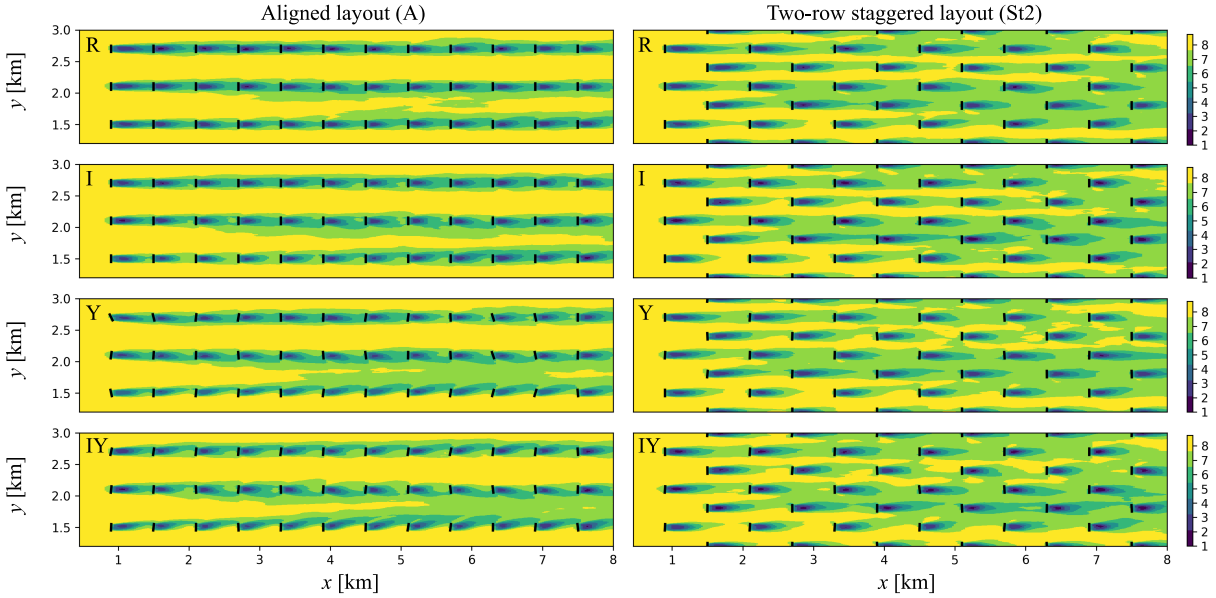

Figure 7: Contours of axial velocity at hub height for widely-spaced wind farms. Turbine rotors are yawed according to the time-averaged turbine yaw angle. *Left:* Aligned layout. *Right:* Two-row staggered layout. *From top to bottom:* Greedy reference control (R), Induction control (I), Yaw control (Y), Combined yaw and induction control (IY). Coloring is in units of m s^{-1}.

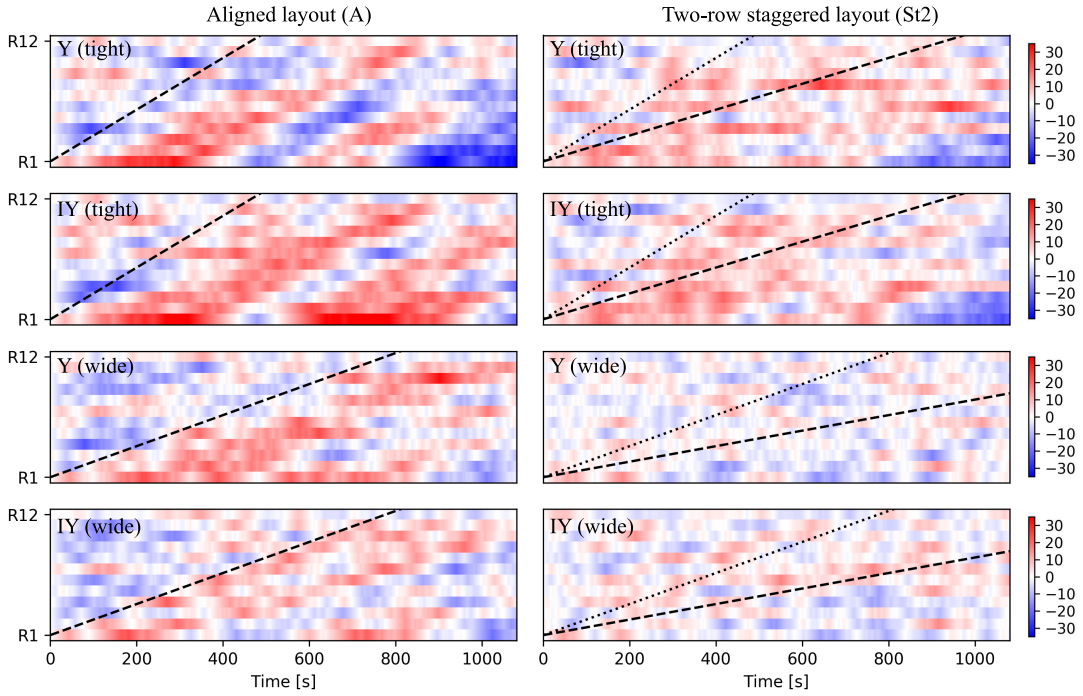

Figure 8: Space-time plot of yaw angles in turbine column at $y \approx 2$ km for yawing control cases I and IY, i.e. every horizontal color data represents yaw angle time series for a single turbine. Dashed (dotted) lines indicate the advection time between axially (diagonally) aligned turbines. Coloring is in units of °.

Acknowledgements

The authors acknowledge funding by the European Research Council (ActiveWindFarms, grant no. 306471). The computational resources and services used in this work were provided by the VSC (Flemish Supercomputer Center), funded by the Research Foundation Flanders (FWO) and the Flemish Government department EWI.

References

[1] J. P. Goit, J. Meyers 2015, 'Optimal control of energy extraction in wind-farm boundary layers', J Fluid Mech 768, 5–50

[2] W. Munters, J. Meyers 2017, 'An optimal control framework for dynamic induction control of wind farms and their interaction with the atmospheric boundary layer', Phil Trans R Soc A 375, 20160100

[3] W. Munters, J. Meyers 2018, 'Towards practical dynamic induction control of wind farms: analysis of optimally controlled wind-farm boundary layers and sinusoidal induction control of first-row turbines', Wind Energ. Sci. Discuss., in review, 2018.

[4] W. Munters, J. Meyers 2018, 'Dynamic Strategies for Yaw and Induction Control of Wind Farms Based on Large-Eddy Simulation and Optimization', Energies 11(1), 177

[5] H. R. Byrd, , P. Lu, J. Nocedal, C. Zhu 1995. 'A limited memory algorithm for bound constrained optimization.' SIAM Journal on Scientific Computing 16(5), 1190-1208

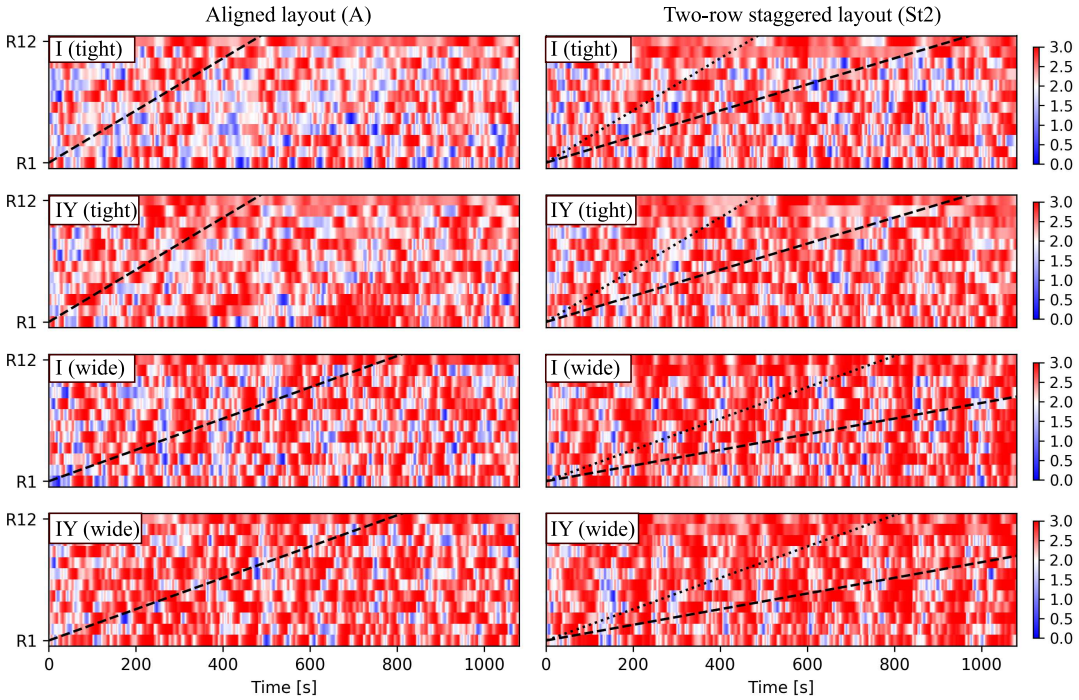

Figure 9: Space-time plot of thrust coefficients in turbine column at $y \approx 2$ km for yawing control cases I and IY, i.e. every horizontal color data represents yaw angle time series for a single turbine. Dashed (dotted) lines indicate the advection time between axially (diagonally) aligned turbines.